AGU PUBLICATIONS

Geochemistry, Geophysics, Geosystems

RESEARCH ARTICLE
10.1002/2016GC006371

Climatic evolution of the central equatorial Pacific since the Last Glacial Maximum

Inah Seo[1], Yuri Lee[2], Yong Il Lee[3], Chan Min Yoo[1], and Kiseong Hyeong[1]

[1]Deep-sea and Seabed Mineral Resources Research Center, Korea Institute of Ocean Science and Technology, Ansan, Republic of Korea, [2]Department of Geology, Kyungpook National University, Daegu, Republic of Korea, [3]School of Earth and Environmental Sciences, Seoul National University, Seoul, Republic of Korea

Key Points:
- Planktic foraminifera reveal oceanographic changes in central equatorial Pacific since the LGM
- The NEC region had expanded equatorward by strengthening of NE Trades during the last deglaciation
- The ITCZ had moved southward at least 2° during the last deglaciation in the central Pacific

Supporting Information:
- Supporting Information S1
- Data Set S1
- Data Set S2

Correspondence to:
K. Hyeong,
kshyeong@kiost.ac.kr

Citation:
Seo, I., Y. Lee, Y. I. Lee, C. M. Yoo, K. Hyeong (2016), Climatic evolution of the central equatorial Pacific since the Last Glacial Maximum, *Geochem. Geophys. Geosyst.*, *17*, 3454–3468, doi:10.1002/2016GC006371.

Received 28 MAR 2016
Accepted 4 AUG 2016
Accepted article online 8 AUG 2016
Published online 27 AUG 2016
Corrected 15 SEPT 2016

This article was corrected on 15 SEPT 2016. See the end of the full text for details.

Abstract This paper investigates paleoceanographic changes at a central equatorial Pacific site (6°40′N, 177°28′W) since the last glacial maximum using planktic foraminifera assemblages, together with the oxygen isotope ($\delta^{18}O$) and Mg/Ca compositions of three species (*Globigerinoides sacculifer*, *Pulleniatina obliquiloculata*, and *Globorotalia tumida*) that dwell in the mixed layer, upper thermocline, and lower thermocline, respectively. While the Mg/Ca-derived temperatures of the mixed layer and lower thermocline varied within a narrow range from 18 ka onward, the upper thermocline temperature increased by as much as 3°C during the last deglaciation (18–12 ka) with a simultaneous decrease of $\delta^{18}O$. These changes are best explained by an enhanced mixing of the upper ocean and a reduced habitat depth separation between *P. obliquiloculata* and *G. sacculifer* during the 18–12 ka interval. The planktic foraminifera assemblage during the same period resembles modern composition at subtropical central Pacific sites that are strongly influenced by the northeasterly Trades and North Equatorial Current (NEC). We suggest that the study site, presently under the control of the Intertropical Convergence Zone (ITCZ)-North Equatorial Countercurrent, had been influenced by the northeasterly Trades and NEC during the 18–12 ka interval. This interpretation is consistent with previous documentation of a more southerly location of the ITCZ during two Northern Hemisphere cooling events; the Heinrich Stadial 1 and the Younger Dryas, and implies that the mean annual position of the ITCZ was located south of the study site, by at least 2° of latitude.

1. Introduction

During the last deglaciation (ca. 18–12 ka), which separated the last glacial maximum (LGM) from the Holocene, warming has occurred in diverse trends and magnitudes depending on sites (Figures 1a and 2). On millennial scales, abrupt cooling and warming events have been observed in the Northern Hemisphere (NH): Heinrich Stadial 1 (HS1; ca. 18–15 ka), Bølling-Allerød (B/A; ca. 15–13 ka), and the Younger Dryas (YD; ca. 13–11.5 ka) [*Bard et al*., 2000; *Hemming*, 2004; *Shakun et al*., 2012, and references therein]. In contrast, temperature fluctuations in the Southern Hemisphere (SH) were rather gradual and revealed a quasi-out-of-phase relationship with their NH counterparts (Figure 2a) [*Bianchi and Gersonde*, 2004; *Kaplan et al*., 2010; *Lamy et al*., 2007].

In the tropical Pacific, deglacial warming reconstruction shows either NH or SH characteristics depending on location, most probably caused by a combination of seasonal biases within the SST proxies (i.e., alkenone and foraminifera Mg/Ca) [*Timmermann et al*., 2014], differences in coastal/equatorial upwelling [*Calvo et al*., 2011; *Kienast et al*., 2006], and regional monsoon patterns [*Huang et al*., 1997; *Oppo and Sun*, 2005] (Figures 2b and 2c). In addition, climatic anomalies reported in the tropical Pacific, such as reduced river runoff and weaker Asian and stronger Australian summer monsoon systems, have been attributed mainly to the southward migration of the Intertropical Convergence Zone (ITCZ), a maximum tropical precipitation belt that results from the convergence of the northeasterly and southeasterly trade winds, during HS1 and YD events [*Ayliffe et al*., 2013; *Gibbons et al*., 2014; *Leduc et al*., 2009; *Mohtadi et al*., 2011a; *Partin et al*., 2007; *Wang et al*., 2001]. Thus, the latitudinal displacement of the ITCZ during these episodes cannot be excluded as a cause of inconsistent warming trends [*Gibbons et al*., 2014; *McGee et al*., 2014] since changes in the strength of the northeasterly and southeasterly trade winds would have resulted in diverse responses in regional precipitation and upwelling patterns in the tropics.

Previous studies of tropical deglacial warming and ITCZ location have been carried out mainly in the western and eastern boundary regions of the Pacific [*Ayliffe et al*., 2013; *Gibbons et al*., 2014; *Leduc et al*., 2009;

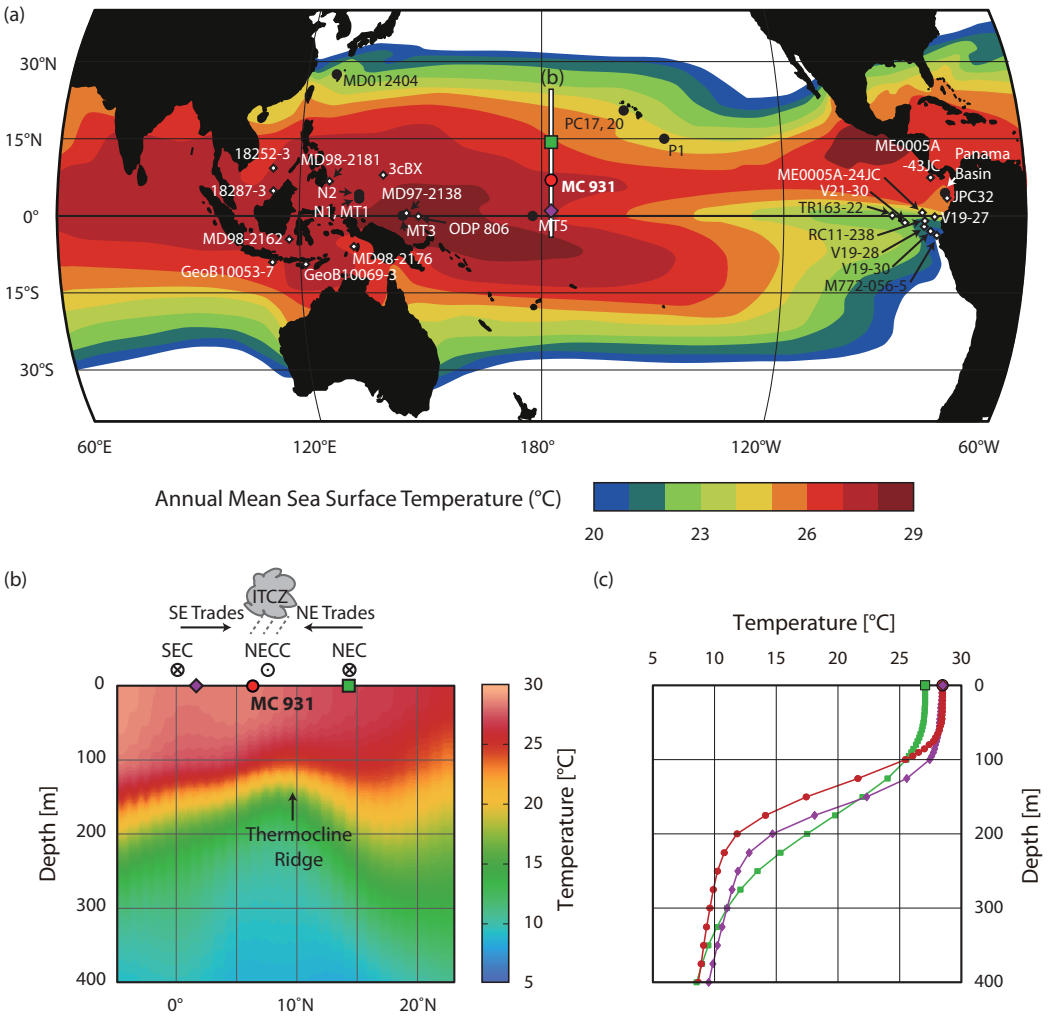

Figure 1. (a) Locations of the study site (MC 931), cores where the paleo-SST and paleo-ITCZ records were reconstructed (diamonds), and sites with planktic foraminifera species assemblage data available (solid circles) discussed in the text. (b) Temperature profile along the 177.5°W transect between 10°S and 22.5°N and (c) depth profile of temperature at 1.5°N, 6.5°N, and 14.5°N (purple diamond, red circle, and green square, respectively) along the 177°W transect. Temperature data are from World Ocean Atlas 2013 [*Locarnini et al*., 2013; *Zweng et al*., 2013].

Mohtadi et al., 2011a; *Partin et al*., 2007; *Wang et al*., 2001] where regional precipitation and upwelling patterns are strongly coupled with ITCZ movement (Figure 2d). Thus, decoupling the consequences of these factors is commonly challenging in these regions. To date, few studies have attempted to interpret deglacial SST evolution in terms of the migration of the ITCZ. *Kienast et al*. [2013] did interpret the systematic changes in meridional SST gradients in the Eastern Equatorial Pacific (EEP) during the last deglaciation in terms of ITCZ migration. However, there have been no field studies to reconstruct the latitudinal extent of the ITCZ displacement during the last deglaciation in the central Pacific region where the coastal upwelling and regional monsoonal effects are minimal.

This study aims to describe and interpret climate evolution in the eastern boundary region of the western Pacific warm pool (WPWP) in the central equatorial Pacific over the last 23 kyrs in terms of the influence of the ITCZ. At present, the central equatorial Pacific near the international dateline is characterized by the narrowest seasonal migration belt of the ITCZ [*Legates and Willmott*, 1990; *Spencer*, 1993]. In contrast, the annual average position of the ITCZ shows the largest meridional displacement in response to a given change in interhemispheric thermal contrast in the modern ocean [*McGee et al*., 2014]. These characteristics of the study site facilitate tracking the migration of the ITCZ in the past with minimal continental effects. Here we investigate temporal variations in temperature and water column structure in the upper ocean using the

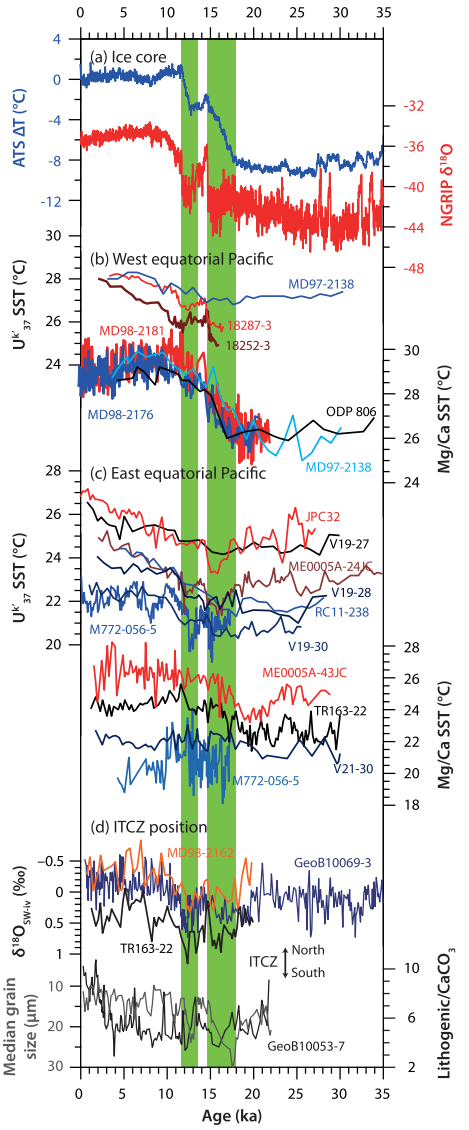

Figure 2. Compilation of published data set showing the last deglacial climate change. (a) Air temperatures from Greenland (NGRIP $\delta^{18}O$ on GICC05 × 1.0063 chronology [North Greenland Ice Core Project members, 2004]) and Antarctica ice cores (Antarctic Temperature Stack (ATS) [*Parrenin et al*., 2013] in degrees Celsius relative to the present day on AICC12 × 1.0063 chronology [*Veres et al*., 2013]). (b) Records of $U^{K'}_{37}$ and foraminifera Mg/Ca-SST in the west equatorial Pacific [*de Garidel-Thoron et al*., 2007; *Kienast et al*., 2001; *Medina-Elizalde and Lea*, 2005; *Stott et al*., 2007] and (c) in the east equatorial Pacific [*Benway et al*., 2006; *Kienast et al*., 2006; *Koutavas and Sachs*, 2008; *Lea et al*., 2006; *Nürnberg et al*., 2015; *Pahnke et al*., 2007]. (d) Reconstructions of the ITCZ position based on the seawater oxygen isotope composition corrected for the global ice volume change ($\delta^{18}O_{sw\text{-}iv}$) from the Eastern Indian Ocean (blue line) [*Gibbons et al*., 2014], East equatorial Pacific (black line) [*Gibbons et al*., 2014; *Lea et al*., 2006] and Western Pacific Warm Pool (orange line) [*Gibbons et al*., 2014; *Visser et al*., 2003] and based on the precipitation records offshore southern Java [*Mohtadi et al*., 2011a].

shell oxygen isotopic composition ($\delta^{18}O$) and Mg/Ca ratios of three planktic foraminifera species (*Globigerinoides sacculifer*, *Pulleniatina obliquiloculata*, and *Globorotalia tumida*), which live at different depth ranges within the water column. As proven in the central WPWP region by *Sagawa et al*. [2012], this multispecies approach will help us to interpret the evolution of temperature gradients between the surface and lower part of the thermocline. In addition, faunal assemblages of planktic foraminifera are analyzed to examine the temporal evolution of the surface ocean environment in terms of ITCZ movement. This study reports proxy data for the past 23 kyrs in the central equatorial Pacific region for the first time, and also addresses the approximate latitudinal extent of the ITCZ displacement and the subsequent response of the upper water column in the central equatorial Pacific during the last deglaciation.

2. Study Site

Sediment core MC 931 (31 cm long) was recovered using a multiple corer from the Magellan Rise in the central equatorial Pacific (6°40′N, 177°28′W; 3365 m depth) during the NAP0903 cruise carried out by the Korea Institute of Ocean Science and Technology (KIOST) in 2009 (Figure 1a). At present, the surface ocean environment at the study site shows small intra-annual variations. The elevated topography of the Magellan Rise, which is about 2000 m shallower than the surrounding basin, allows for good preservation of calcareous microfossils in association with relatively high rates of accumulation and prevents syndepositional or postdepositional processes caused by lateral advection. The sediment core was composed predominantly of calcareous ooze that contained ~90% carbonate, and did not show any identifiable down-core changes in lithology.

The North Equatorial Countercurrent (NECC), which has a location coupled with the ITCZ [*Donguy and Meyers*, 1996; *Masunaga and L'Ecuyer*, 2010], flows over the site of the sediment core and transports warm and low-nutrient surface water to the study site from the WPWP (Figure 1b). South of the study site, the westward-flowing South Equatorial Current (SEC) prevails (Figure 1b). Southeasterly trade winds induce upwelling and bring nutrients to the surface at the equator, resulting in higher primary production than in the WPWP and NECC regions [*Eldin and Rodier*, 2003; *Le Bouteiller et al*., 2003]. The area to the north of the study site is influenced by the North Equatorial Current (NEC) and strong northeasterly trade winds (Figure 1b). The boundary region between the NECC and NEC is defined by the thermocline ridge (7°N–9°N)

where the eastward/westward-flowing surface currents induce curl-driven upwelling (Figure 1b). The seawater temperature profiles representing SEC, NECC, and NEC regions along the 177.5°W (1.5°N, 6.5°N, and 14.5°N, respectively) reflect vertical water column structures resulted from these surface current and wind patterns (Figures 1b and 1c).

3. Analytical Methods

Core MC 931 was subsampled at an interval of 1 cm, and these subsamples were freeze-dried and stored in plastic bottles in a cool room. Planktic foraminifera assemblages were determined with at least 300 foraminifer specimens picked from the >125 μm fraction of each sample. The foraminifera species were identified based on *Kennett and Srinivasan* [1983], *Saitō et al*. [1981], and *Ujiie and Ujiie* [2000].

The chronology of the core was established from the 5–6, 11–12, 13–14, 20–21, and 30–31 cm intervals using ^{14}C measurements of mixed species of planktic foraminifera. ^{14}C was analyzed within an error range of less than 60 years using the accelerator mass spectrometry (AMS) technique at the Beta Analytic Radiocarbon Dating Laboratory, USA. The measured radiocarbon ages were corrected for isotopic fractionation and calibrated to calendar years before present (Cal ^{14}C age) using Calib v. 7.0 software [*Stuiver and Reimer*, 1993]. This correction was based on the Marine13 data set [*Reimer et al*., 2013] and a local reservoir effect (ΔR) of 9 ± 5 years [*Guilderson et al*., 1998].

Three planktic foraminifera species, *G. sacculifer* (without final sac, 250–355 μm,), *P. obliquiloculata* (355–425 μm), and *G. tumida* (355–425 μm), were analyzed for δ^{18}O and Mg/Ca ratios. Stable oxygen isotope compositions (δ^{18}O) were determined using a Finnigan MAT 251 mass spectrometer at the University of Michigan at Ann Arbor, USA. About 20, 10, and 8 specimens of *G. sacculifer*, *P. obliquiloculata*, and *G. tumida*, respectively, were analyzed. The 1σ standard deviation of repeat analyses of the reference material (NBS-19; National Bureau of Standards) was 0.09‰ ($n = 24$). Mg/Ca ratios were determined using an inductively coupled plasma-optical emission spectrophotometer (ICP-OES; Perkin-Elmer Optima 3300 DV) at the Korea Institute of Ocean Science and Technology, Ansan, Korea. For the Mg/Ca measurements, following *Barker et al*. [2003], 20–30 monospecific tests were crushed and homogenized, and subsequently cleaned with methanol (clay removal), NaOH-buffered hydrogen peroxide (removal of organic matter), and 0.001 N nitric acid (removal of high-Mg calcite). The concentrations of Ca and Mg were measured from the spectral lines at 407.776 and 279.553 nm, respectively. Instrumental drift was corrected according to *Schrag* [1999] and *Marcos and Hill* [2000]. The ECRM 752-1 standard (Bureau of Analyzed Samples) was analyzed twice for every three samples and the results were used for correction of measured sample Mg/Ca ratios. Replicate measurements on 91 samples revealed an average standard deviation of 0.16 mmol/mol, giving corresponding error of ±1.6°C [*Mohtadi et al*., 2014].

To predict the δ^{18}O of planktic foraminifer species inhabiting various depths, the calcite δ^{18}O-depth relationship was established at the study site using the theoretical equation that links the δ^{18}O of seawater with temperature [*Kim and O'Neil*, 1997]. For this equation, the δ^{18}O of seawater is calculated from the salinity-δ^{18}O relationship of surface and subsurface water in the central tropical Pacific [*Conroy et al*., 2014], and the optimum interpolation temperature and salinity were taken from the World Ocean Atlas 2013 [*Locarnini et al*., 2013; *Zweng et al*., 2013]. The calcification depths of three planktic foraminifera species of interest at the study site were estimated based on the $\delta^{18}O_{calcite}$ calculated at 6.5°N, 177.5°W (Figure 3).

The calcification temperature (T) of planktic foraminifera is often expressed as $\mathrm{Mg/Ca} = b \times \exp(a \times T)$ [*Lea et al*., 1999; *Nürnberg et al*., 1996]. Since we picked *G. sacculifer* specimens from 250 to 355 μm size fraction, smaller than that is generally used for the paleo-SST reconstruction (355–500 μm) [e.g., *Anand et al*., 2003; *Mohtadi et al*., 2011b], calibration coefficients ($a = 0.090 \pm 0.013$, $b = 0.37 \pm 0.03$) were adopted from *Dekens et al*. [2002] which were derived from the same size fraction. For *P. obliquiloculata* ($a = 0.090 \pm 0.003$, $b = 0.328 \pm 0.007$) and *G. tumida* ($a = 0.09$, $b = 0.53$; error ranges are not available), calibration coefficients were adopted from *Anand et al*. [2003] and *Rickaby and Halloran* [2005], respectively.

4. Results

The age model of core MC 931 was established based on the ^{14}C measurements (supporting information Table S1). Average sedimentation rate at the core site for the last 23 kyr is 1.35 cm/kyr, which covers the entire last deglaciation.

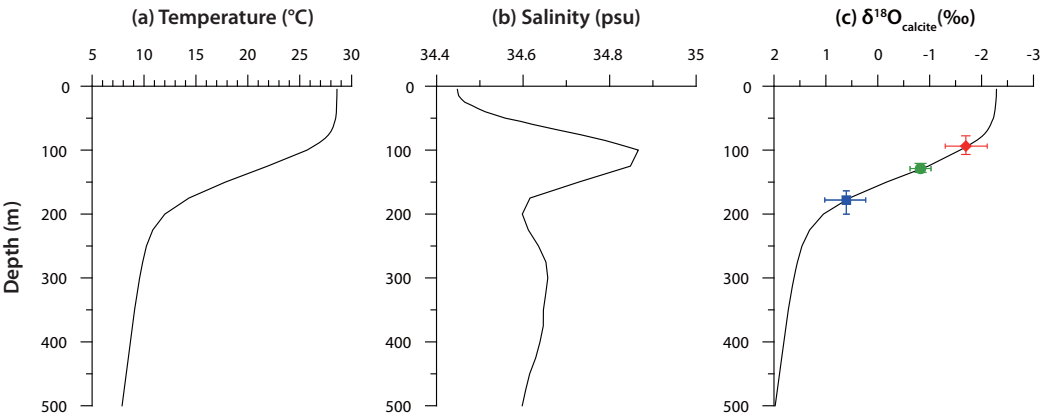

Figure 3. Depth profile of annual mean of optimum interpolated (OI) temperature (a) and salinity (b) records provided in World Ocean Atlas 2013 [*Locarnini et al.*, 2013; *Zweng et al.*, 2013]. (c) The estimated calcification depths of three species by comparison of an average δ^{18}O composition of late Holocene (<6 ka) planktic foraminifera species with the predicted calcite δ^{18}O (see text for details): *G. sacculifer* (red), *P. obliquiloculata* (green), and *G. tumida* (blue).

The down-core δ^{18}O and Mg/Ca results from the three species are shown in Figures 4a and 4b, respectively (supporting information Table S1). For the late Holocene (0–6 ka), the δ^{18}O composition of *G. sacculifer* ($-1.66 \pm 0.46‰$; $n = 5$, 1σ), *P. obliquiloculata* ($-0.86 \pm 0.20‰$; $n = 5$, 1σ), and *G. tumida* ($0.56 \pm 0.46‰$; $n = 5$, 1σ) are in general agreement with previously reported values from the center of the WPWP [*Sagawa et al.*, 2012], but with some minor offsets that we suggest to reflect temperature and salinity differences between the two sites. For the same period (0–6 ka), the determined Mg/Ca ratios of *G. sacculifer* (4.15 ± 0.14 mmol/mol; $n = 5$, 1σ) and *G. tumida* (1.85 ± 0.11 mmol/mol; $n = 5$) are similar to those at the WPWP center (ca. 4.0 and ca. 1.6 mmol/mol, respectively; data not shown), but those of *P. obliquiloculata*

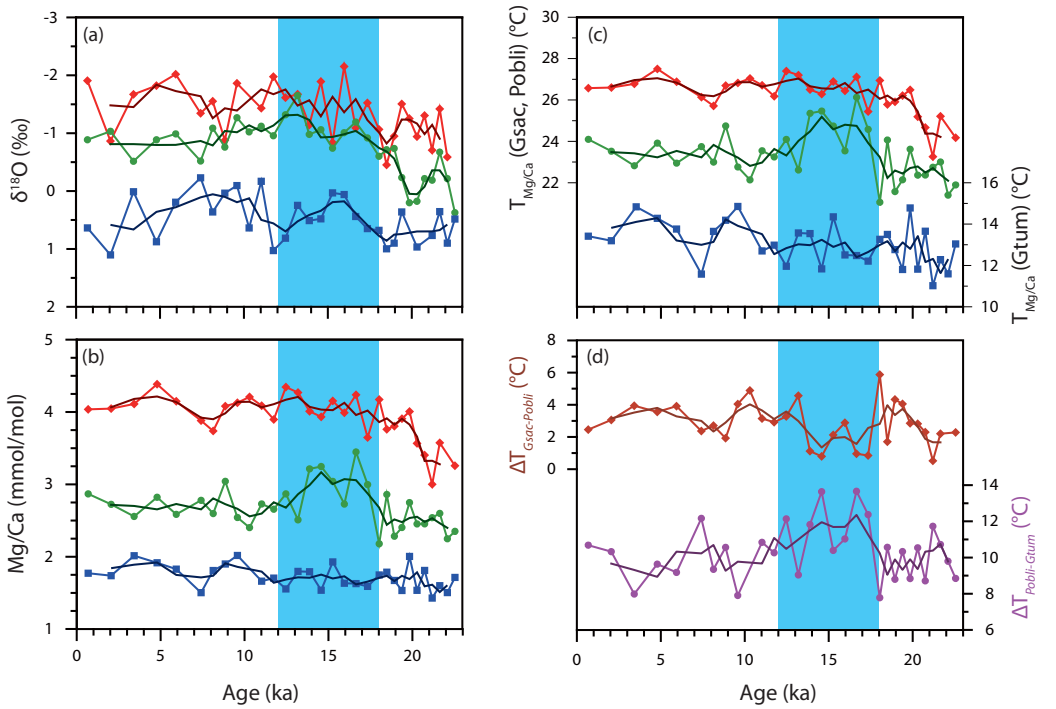

Figure 4. Analytical results of δ^{18}O (a) and Mg/Ca (b) compositions of *G. sacculifer* (red diamonds), *P. obliquiloculata* (green circles), and *G. tumida* (blue squares), and (c) Mg/Ca-derived calcification temperatures converted using equations provided by *Dekens et al.* [2002], *Anand et al.* [2003], and *Rickaby and Halloran* [2005] in MC 931. (d) Temperature differences between *G. sacculifer* and *P. obliquiloculata* (brown diamonds) and between *P. obliquiloculata* and *G. tumida* (purple circles). Light blue shades mark the time interval with reduced compositional gradient between species.

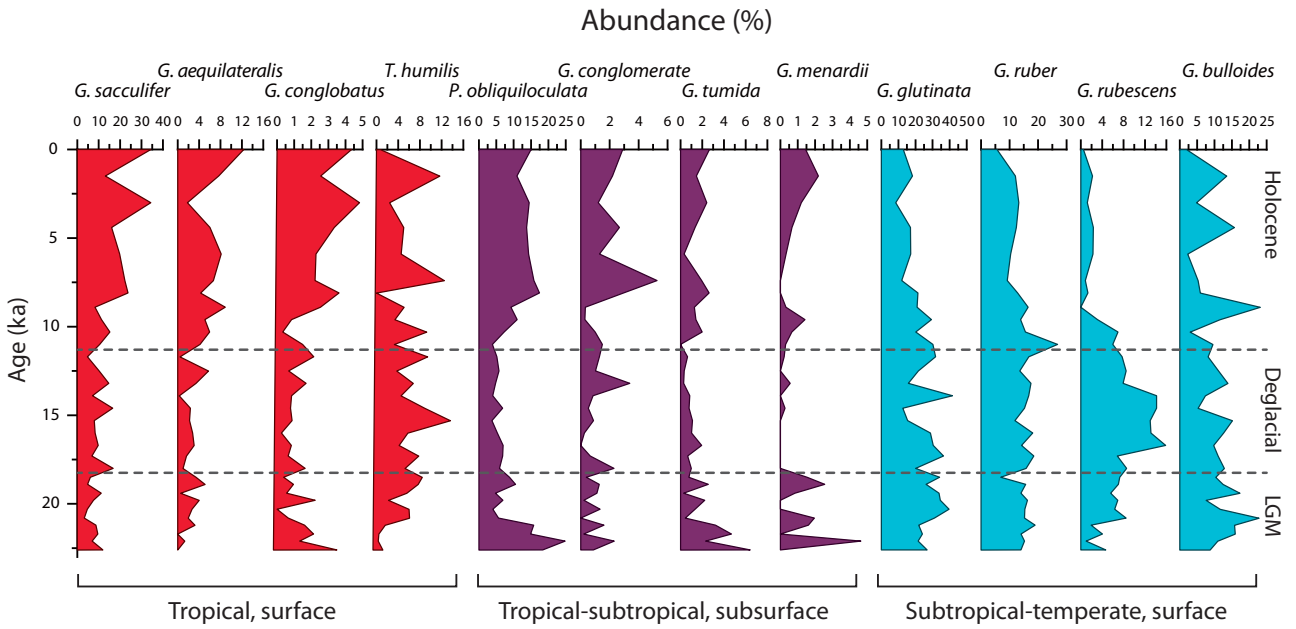

Figure 5. Faunal assemblage of major planktic foraminifera species in MC 931.

(2.71 ± 0.14. mmol/mol; $n = 31$, 1σ) are higher than those at the WPWP center (ca. 2.3 mmol/mol; data not shown) [*Sagawa et al*., 2012].

Thirty-four species of planktic foraminifera were identified in the sample core, but it was composed mainly of the tropical-subtropical planktic foraminifer species *G. glutinata*, *G. ruber*, *G. sacculifer*, and *G. bulloides*, with relative abundances of 24.8%, 14.6%, 12.5%, and 10.9%, respectively (supporting information Table S2). Figure 5 shows temporal changes in the relative abundances of the 12 major species.

5. Discussion

5.1. Reliability of Foraminifera Calcification Depth and Temperature Estimates

G. sacculifer is known to inhabit the upper 80 m of the water column, but its depth preference varies with its growth stage and size [*Bijma and Hemleben*, 1994]. In the early stages of growth, *G. sacculifer* lives in the upper photic zone (0–50 m depth) [*Anand et al*., 2003; *Bijma and Hemleben*, 1994; *Hemleben et al*., 1987] but inhabits greater depths during its adult stage [*Bé*, 1980; *Bijma and Hemleben*, 1994]. *P. obliquiloculata* lives in the lower photic zone-upper thermocline (50–130 m depth), and its calcification temperature varies within a small range [*Anand et al*., 2003; *Rincón-Martínez et al*., 2011; *Sagawa et al*., 2012]. *G. tumida*, a thermocline-dwelling species, calcifies below the seasonal thermocline (100–250 m depth) [*Fairbanks and Wiebe*, 1980; *Farmer et al*., 2007]. Based on the depth habitats of these three species in the WPWP region (3cBX in Figure 1a) estimated by *Sagawa et al*. [2012], we considered that the calcification temperatures and seawater δ^{18}O of the *G. sacculifer*, *P. obliquiloculata*, and *G. tumida* sampled here represented those of the mixed layer, upper thermocline, and lower thermocline, respectively.

Based on the projection of an average late Holocene (<6 ka) δ^{18}O composition of each planktic foraminifera species onto the established calcite δ^{18}O-depth relationship, the calcification depths were estimated to be 70–100 m for *G. sacculifer*, 120–140 m for *P. obliquiloculata*, and 160–200 m for *G. tumida* (Figure 3). The predicted depths are slightly greater than, but largely consistent with, the previously reported depth habitats of the three species estimated in the center of the WPWP; i.e., 40–80 m for *G. sacculifer*, 100–130 m for *P. obliquiloculata*, and 140–180 m depth for *G. tumida* [*Sagawa et al*., 2012].

The Mg/Ca-derived calcification temperatures of the three planktic foraminifera species for the late Holocene (<6 ka) were estimated to be 26.8°C (±0.4), 23.5°C (±0.7), and 12.9°C (±0.8) for *G. sacculifer*, *P. obliquiloculata*, and *G. tumida*, respectively (Figure 4c). These temperatures are encountered at depths of 90, 120, and 190 m, respectively, at the study site at present; thus, the Mg/Ca-derived temperature of each species

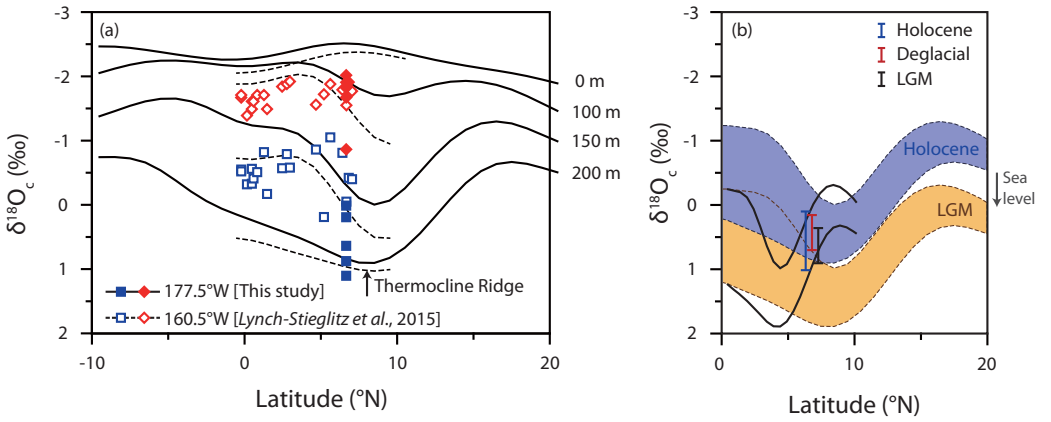

Figure 6. (a) Measured $\delta^{18}O_c$ values for the Holocene *G. sacculifer* (red diamonds) and *G. tumida* (blue squares) at 177.5°W (solid symbols; this study) and along 160.5°W (open symbols) [*Lynch-Stieglitz et al*., 2015]. Expected $\delta^{18}O$ values for calcite ($\delta^{18}O_c$) for various depths (0, 100, 150, and 200 m) are plotted together along 177.5°W (solid lines) and 160.5°W (dashed lines) based on temperature and salinity data from the World Ocean Atlas 2013 [*Locarnini et al*., 2013; *Zweng et al*., 2013]. (b) $\delta^{18}O$ range of *G. tumida* determined in this study for the Holocene (blue), deglaciation (red), and LGM (black) with theoretically estimated $\delta^{18}O_c$ of the 150–200 m depth range for the Holocene (blue shaded zone) and for the LGM (yellow shaded zone). $\delta^{18}O_c$ range of the LGM was constructed by simply adding 1‰ to the Holocene range to account for the sea level drop. Solid line depicts a situation of the meridionally contracted frontal system due to southward migration of the ITCZ with $\delta^{18}O_c$ range for the LGM.

represents that of the mixed layer, upper thermocline, and lower thermocline, respectively (Figure 3). These results are consistent with the aforementioned calcification depths of the three species derived from $\delta^{18}O$: 70–100 m for *G. sacculifer*, 120–140 m for *P. obliquiloculata*, and 160–200 m depth for *G. tumida*. Such consistent results indicate the reliability of the estimated temperatures presented in this study.

At the depth where the study core recovered (3409 m depth) selective dissolution of high-Mg/Ca calcite could have altered the foraminifera Mg/Ca [*Brown and Elderfield*, 1996; *Regenberg et al*., 2014]. However, since the estimated seawater temperatures and habitat depths of target species are similar to those expected from $\delta^{18}O$, the Mg/Ca-derived temperatures are assumed to indicate reliable calcification temperature.

The analyzed $\delta^{18}O$ especially of *G. sacculifer* and *G. tumida* shows considerable fluctuation as much as 1‰ that is unusual compared to data presented in other studies. The study site is located in a frontal region strongly influenced by the ITCZ and wind-driven surface currents such as NECC and NEC (Figure 1b). The divergence between the NECC and NEC causes shoaling of cold subsurface water, which places the thermocline ridge at 7°N–9°N (Figure 1b). These various features create a strong meridional gradient of seawater $\delta^{18}O$ in the upper water column [e.g., *Leech et al*., 2013; *Lynch-Stieglitz et al*., 2015] (Figure 6a). *G. sacculifer* and *G. tumida* from the core top sediments along the 160.5°W transect also show wide variations in $\delta^{18}O$ composition [*Lynch-Stieglitz et al*., 2015]. Especially, *G. tumida* reveals a wide range of $\delta^{18}O$ composition varying in magnitude of over 1‰ between 5°N and 7°N (Figure 6a). The aforementioned observations suggest that relatively larger fluctuations of our $\delta^{18}O$ data could have resulted from the steep vertical and meridional change of water column properties at the study site. Under this oceanographic environment, latitudinal variations in position of surface current system, resulted from climatic variability in seasonal to millennial time scales, could have induced the wide variabilities in $\delta^{18}O$ of surface dwelling foraminifera species. The displacement of a frontal system is associated with changes of salinity and temperature, both of which affect $\delta^{18}O$ of foraminifera. Thus, variability of $\delta^{18}O$ is likely larger, especially when temperature and salinity change induce $\delta^{18}O$ change in same direction, than that of Mg/Ca which is controlled solely by temperature. This process could also be an explanation for lacking of sea level signal in $\delta^{18}O$ of *G. tumida* (Figure 4a) as latitudinal displacement of these systems could create changes in $\delta^{18}O$ of seawater that are similar in magnitude with sea level signal (Figure 6b). In addition, the use of 250–355 μm size fraction for the $\delta^{18}O$ of foraminifera might be partly responsible for large fluctuations of $\delta^{18}O$ as smaller specimens would have recorded oceanographic conditions of shorter period than the larger ones. We used the sample amounts commonly employed for $\delta^{18}O$ measurements; about 20 specimens of *G. sacculifer* and eight specimens of *G. tumida* [e.g., *Mohtadi et al*., 2011a]. However, such sample amounts would not be sufficient to

yield an average composition of a time period of interest at the study location where the steep environmental gradient could induce strong compositional heterogeneity among individual specimens. Despite of large fluctuations, δ^{18}O values of three species averaged for the late Holocene (0–6 ka) are in general agreement with previously reported values from the center of the WPWP [*Sagawa et al*., 2012]. Nevertheless, δ^{18}O values show rather large variability and are only used for the estimation of calcification depth.

5.2. Changes in the Upper Water Column Structure During the Last Deglaciation

Mg/Ca-derived temperatures of the mixed layer and lower thermocline increase gradually from 23 ka, but are relatively constant after 18 ka (Figure 4c). In contrast, the upper thermocline temperatures increased from its LGM value (ca. 22.5°C) by as much as 3°C during the last deglaciation between 18 and 12 ka, but decreased to the present level (ca. 23.5°C) at 12 ka (Figure 4c). This suggests that the vertical temperature gradient between the dwelling depths of *P. obliquiloculata* and *G. sacculifer* was reduced during the 18–12 ka period, but that the gradient between *P. obliquiloculata* and *G. tumida* increased over this period (Figure 4d). These trends recorded during the last deglaciation could have resulted from either an increase in temperature at the dwelling depth and/or a change in habitat depth of *P. obliquiloculata*.

The increase in deglacial subsurface water temperature could have been generated by the warming of the thermocline water mass. Indeed, warming of intermediate water that upwells in the equatorial region is indicated by several reconstructions of the last deglaciation period [*Bostock et al*., 2013; *Bova et al*., 2015; *Calvo et al*., 2007; *Nürnberg et al*., 2015]. Likewise, other studies suggest that the spatial extent of equatorial upwelling region expanded westward and southward during the last deglacial period [*Kubota et al*., 2014; *Palmer and Pearson*, 2003]. Thus, warming of thermocline water could have occurred by upwelling at the study site during this time period. However, this hypothesis of sequential warming from the deep thermostad to the thermocline water cannot be applied to the study site. If this had been the case, the lower thermocline temperature, represented by the Mg/Ca ratio of *G. tumida*, should have increased simultaneously with that of the upper thermocline, yet it remained stable throughout the study period (Figure 4c). Despite the increases in the temperature of air [*Parrenin et al*., 2013], surface ocean [*Lamy et al*., 2004; *Mohtadi et al*., 2008; *Romero et al*., 2006], and intermediate water that upwelled at the EEP [*Bova et al*., 2015] in the SH at this time, the southern sourced intermediate water did not reach as far north as at the core site just as today or the well-developed thick mixed layer or weak upwelling to the north of the equator could have prevented the penetration of SH-sourced intermediate water to the upper ocean at the study site.

Interestingly, the difference in δ^{18}O compositions between *G. sacculifer* and *P. obliquiloculata* decreased simultaneously with those of the Mg/Ca-derived temperatures between 18 and 12 ka (Figure 4). This suggests that the increase in the calcification temperature of *P. obliquiloculata* was accompanied by a shoaling of the maximum population depth of *P. obliquiloculata* during this period. Although *P. obliquiloculata* occurs mainly in tropical-subtropical subsurface waters at depths of 60–150 m [*Cléroux et al*., 2008; *Erez and Honjo*, 1981; *Farmer et al*., 2007], previous studies indicated wide variations in its habitat depth. In the tropical Pacific, for example, the maximum population depth range of *P. obliquiloculata* was estimated to be 100–140 m from its δ^{18}O composition in the western Pacific [*Patrick and Thunell*, 1997; *Sagawa et al*., 2012; this study], but 30–100 m in the eastern Pacific [*Rincón-Martínez et al*., 2011]. Similar depth habitat variation has also been reported for other thermocline-dwelling species (*Globorotalia menardii* and *Neogloboquadrina dutetrei*) across the tropical Pacific [*Patrick and Thunell*, 1997]. In particular, the depth habitats of *G. sacculifer* and *P. obliquiloculata* were reported as being indistinguishable in the tropical eastern Pacific [*Rincón-Martínez et al*., 2011].

The inability to separate the depth habitats of these two foraminiferal species in the EEP is probably related to the upper ocean conditions in the EEP. The density gradient in the EEP region is less steep than its western counterpart, which makes the water column structure and vertical zonation of planktic foraminiferal habitats unstable and the separation of depth habitats between species can be reduced in the upper ocean [*Caromel et al*., 2014; *Coxall et al*., 2000; *Rashid and Boyle*, 2007]. Thus, the depth habitat of *P. obliquiloculata* at the study site could have overlapped with that of *G. sacculifer* under such conditions. The lower-thermocline inhabiting species, *G. tumida*, is known to dwell below the photic zone, mostly deeper than 100–150 m, and therefore does not show strong spatial variations in habitat depth [*Rincón-Martínez et al*., 2011; *Sagawa et al*., 2012]. Consequently, between 18 and 12 ka the increase in the calcification temperature of *P. obliquiloculata*, which was unique among the three species studied here, was most probably

caused by a shoaling of the depth habitat, which suggests an enhanced surface ocean mixing at the study site at this time. Enhanced surface mixing would have resulted in deepening of thermocline and smaller temperature gradient in the mixed layer, which could have been an aid to induce the decrease in differences of Mg/Ca and $\delta^{18}O$ between *G. sacculifer* and *P. obliquiloculata* with minimal change in the habitat depth of *P. obliquiloculata*.

5.3. Southward Displacement of the NEC During the Last Deglaciation

Changes in the upper ocean stratification between 18 and 12 ka, but without any associated warming of the deep thermocline water, could have been caused by enhanced wind-driven mixing. Today, the study site is positioned beneath the ITCZ and is characterized by high precipitation, light winds, and buoyant surface water mass. The meridional displacement of the ITCZ from its present position would have exposed the site to the influence of either the northeasterly or southeasterly trades, which would have led to enhanced mixing of the surface water column. It would also have reduced the degree of stratification of the upper water column by placing the site outside of the zone of intense precipitation.

As faunal assemblage of planktic foraminifera in the tropical Pacific Ocean is strongly affected by surface ocean structure and thermocline depths [*Andreasen and Ravelo*, 1997], changes in the upper ocean structure due to the migration of the ITCZ should have been recorded in faunal assemblages of the study site. However, faunal assemblage data can be used reliably with the basic premise that it was not significantly modified from the depositional equivalents by dissolution. Dissolution-susceptible species could have been dissolved out preferentially after deposition at the period of intensified carbonate dissolution such as the late Holocene [*Kimoto et al*., 2003; *Le and Thunell*, 1996; *Thunell and Honjo*, 1981a], which may result in a faunal composition overestimating the abundance of dissolution-resistant species in a record. However, the planktic foraminifera assemblage of the late Holocene at the study site is similar to those reported from sediment trap studies (no effect of dissolution) at nearby stations (e.g., MT1, MT3, and MT5). Especially, contents of *G. rubescens*, one of the most dissolution-susceptible species, in the center of WPWP ($<$1% at MT1 and MT3 sites) and central equatorial Pacific ($\sim$2.6% in average at MT5) are well compared to our late Holocene data (0.5–2.3%), indicating minimal influence of dissolution-induced faunal composition changes at the study site. Moreover, planktic foraminifera assemblages during the last deglaciation, the period of most enhanced carbonate preservation since the LGM [*Berger*, 1977; *Mekik et al*., 2012], are characterized by high abundance of *G. rubescens* (6.8–15.9%). Such a high abundance is only reported in a sediment trap study carried out in a north central Pacific site (23%, station P1) [*Thunell and Honjo*, 1981b]. We therefore conclude that the change in faunal assemblage is primarily induced by the environmental change associated with climate evolution since the LGM at the study site.

The temporal change in faunal assemblages of planktic foraminifera suggests the influence of NEC to the study site, likely associated with southward displacement of the ITCZ during the last deglaciation. The foraminifera in the core were dominated by tropical-subtropical species (e.g., *G. glutinata*, *G. ruber*, *G. sacculifer*, *P. obliquiloculata*, and *G. rubescens*) over the past 23 kyrs, but with increased relative abundances of warm oligotrophic WPWP species (e.g., *G. sacculifer*, *G. aequilateralis*, and *P. obliquiloculata*) during the Holocene (Figure 5). As a general trend, the increased abundance (51%) of *G. ruber*, *G. glutinata*, and *G. rubescens* during the last deglaciation (ca. 18–12 ka) compared with that (27%) of the late Holocene (0–6 ka) is noteworthy. Although these species generally inhabit warm tropical-subtropical ocean [*Black et al*., 2001; *Hemleben et al*., 1989; *Thunell and Reynolds*, 1984], they are able to adapt to a cooler ocean environment than the warm pool species such as *G. sacculifer*, *G. aequilateralis*, and *P. obliquiloculata* [*Riforgiato*, 2013; *Yamasaki et al*., 2008]. In particular, *G. rubescens* is not commonly found in the tropical Pacific at present (e.g., $<$1% in all the WPWP sites, N1, N2, MT1, and MT3, and 2.6% at the equatorial site MT5) [*Kawahata et al*., 2002; *Yamasaki et al*., 2008], but has been reported as a significant component in a sediment trap (23%, Station P1, ca. 15°N) and surface sediments (5.6%, PC17 and PC20, ca. 21°N) from the subtropical central Pacific near the Hawaiian Islands (see locations in Figure 1a) [*Lee et al*., 2001; *Thunell and Honjo*, 1981]. The spatial distribution of *G. rubescens* indicates its preference to more off-equatorial oligotrophic ocean conditions. Our site reveals relatively high abundances of *G. rubescens* varying from 6.8% to 16.8% (10.6% on average) during the last deglaciation period, which is well compared to those of the NEC region at present. Therefore, we suggest that our site experienced environmental conditions during the last deglaciation similar to those of the present day NEC region.

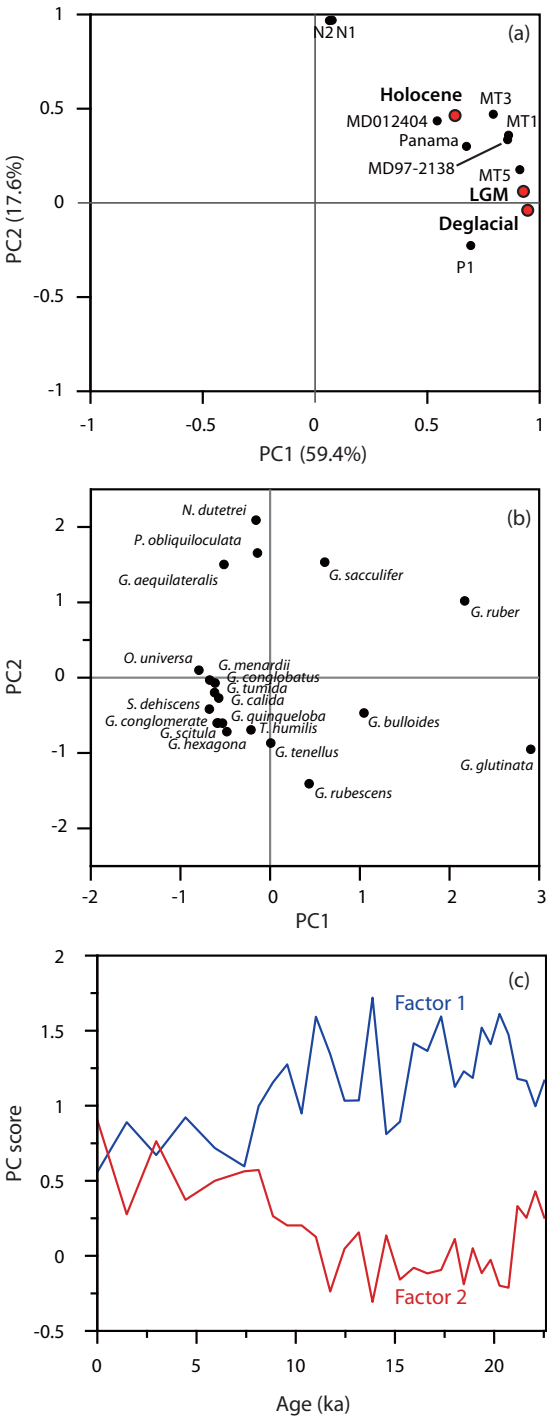

Figure 7. Results of principal component (PC) analyses on planktic foraminifera assemblage data from the study site and other tropical-subtropical Pacific sites determined for sediment trap and Holocene core samples (see locations in Figure 1a) [*Chang et al*., 2008; *Kawahata et al*., 2002; *Thunell and Honjo*, 1981a; *Thunell and Reynolds*, 1984; *Yamasaki et al*., 2008]. (a) PC scores of the study site (red: Holocene, last deglaciation and LGM) and other tropical-subtropical sites (black), (b) PC loadings of planktic foraminifera species, and (c) temporal changes of scores of factor 1 and 2 in MC931.

To assess the statistical similarity in planktic foraminifera assemblages, we carried out a principal component analysis (PCA) for the average value of the Holocene (<6 ka), last deglaciation (12–18 ka) and LGM (19–23 ka), and previously reported Holocene data over the tropical-subtropical Pacific (see locations in Figure 1a) using SPSS program ver. 23. Principal component (PC) 1 (59.4%) and 2 (17.6%) accounted for 77.0% of the total variance after Varimax rotation (Figure 7a). Interestingly, deglacial composition of MC 931 shows closer resemblance to that of a subtropical P1 site (Figure 7a); i.e., the dominance of *G. ruber* over *G. sacculifer* and the common occurrence of *G. rubescens* and/or *G. glutinata* [*Thunell and Honjo*, 1981a] (Figure 5). In contrast, faunal assemblage of the study site during the Holocene is projected in between those of MT1, 3, and 5 collected in the La Nina year [*Yamazaki et al*., 2008] and N1 and 2 collected in the El Nino year in the WPWP [*Kawahata et al*., 2002]. It is consistent with environmental setting of the study site at present locating at eastern margin of the WPWP. Even though the faunal assemblage of planktic foraminifera in the WPWP region is based on the 1 year long sediment trap data sets, the close projection of the faunal assemblages of our Holocene sample and the trap sample collected during the El Nino year (MT1, MT3, and MT5) [*Yamazaki et al*., 2008] as well as during the La Nina year (N1 and N2) [*Kawahata et al*., 2002] indicates the representativeness of the sediment trap data despite the strong interannual variability. Faunal composition of the LGM shows an intermediate values between those of deglacial and MT5 from the equatorial upwelling region. Close projection of MD012404 (26°39′N, 125°49′E) and Panama Basin (5°21′N, 81°53′W) to our Holocene data is a statistical caveat caused by high PC1 and PC2 loadings from *N. dutertrei* and *G. bulloides* rather than similarities in faunal assemblages (Figures 7a and 7b).

Based on the PC scores of the sites and loadings of planktic foraminifera species (Figures 7a and 7b), PC1 and PC2 can be interpreted to represent the less stratified subtropical and the more stratified tropical surface ocean conditions, respectively. From the PC loadings of each foraminifera species (Figure 7b), the high abundance of *G. ruber* and *G. glutinata* is likely responsible for the high score of PC1 during the last deglaciation at the study site (Figure 7c). High scores of PC1 with the corresponding lower scores of PC2 during the last deglaciation suggest the prevalence of subtropical condition at the study site (Figure 7c). Thus, we

postulate that the surface ocean conditions at the study site during the last deglaciation were similar to those of the NEC region at present, where the surface ocean conditions are affected by strong northeasterly trade winds and characterized by weaker upper ocean stratification (Figures 1b and 1c).

5.4. Causes for Southward Migration of the ITCZ During the Last Deglaciation

Based on the temporal changes in water column structure and faunal assemblages at the study site, we conclude that the surface ocean condition during the last deglaciation was strongly influenced by northeasterly trade winds and the NEC, which can be attributed to displacement of the ITCZ and NECC to the south of the study site. Such phenomenon was likely resulted from the interhemispheric difference in deglacial warming. For the last deglacial period, the early warming of the SH high latitudes relative to their NH counterpart [see *Denton et al*., 2010, and references therein] resulted in a decreased pole-to-equator temperature gradient in the SH. In particular, the interhemispheric thermal asymmetry between the SH and NH was significantly intensified during the NH cooling events (i.e., HS1 and YD) [*Barker et al*., 2009; *Denton et al*., 2010; *McGee et al*., 2014; *Shakun et al*., 2012; *Stenni et al*., 2011]. Such strong asymmetric high-latitude thermal forcing requires an energy balance that was accomplished by the southward displacement of the ITCZ, as has been suggested in many reconstructions [*Haug et al*., 2001; *Mohtadi et al*., 2011a; *Montade et al*., 2015; *Peterson et al*., 2000] and model simulations [*Gibbons et al*., 2014; *McGee et al*., 2014; *Mohtadi et al*., 2014]. These studies suggesting the southward shift of the ITCZ and strengthening of the northeasterly trade winds strongly support our inference that the ITCZ was located south of the study site during the last deglaciation. As a result, the study site was most probably under the influence of intensified northeasterly trade winds, which led to a less stratified upper ocean structure because of wind-driven mixing. Our study do not resolve the Bølling-Allerød episode (ca. 15–13 ka), a brief NH warming that occurred between the HS1 and YD events (Figure 4). Instead, our Mg/Ca record of *P. obliquiloculata* and the abundance of *G. rubescens* show a broad bulge between 18 and 12 ka when these three events occurred. This lack of detail is caused by the low temporal resolution (ca. 1 ka) of our data, which is too coarse to resolve such short-term variability. After 12 ka, the upper ocean at the study site might have been stratified to the present level by the reduced interhemispheric thermal contrast and resultant northward migration of the ITCZ to its present position. Accordingly, we suggest that the present oceanographic and atmospheric conditions of the study site, influenced by the ITCZ and NECC, have been persisting since 12 ka.

The surface ocean condition during the LGM is interpreted having been in between those of off-equatorial oligotrophic condition of the deglaciation and the WPWP condition of the present, which is inferred from Mg/Ca records showing greater difference during the LGM than the deglacial period (Figure 4c) and foraminifera assemblage indicating surface ocean condition in between those of off-equatorial oligotrophic and the WPWP conditions (Figure 7). This interpretation is consistent with the simulation result of *McGee et al*. [2014], in which inter-hemispheric thermal contrasts during the LGM indicated the average ITCZ position in between those during the last deglaciation and of the present.

It is not possible to test for the full latitudinal extent of ITCZ migration during the last deglaciation period using our data derived from a single site, but we can place a lower limit on its overall extent in the region using the faunal assemblages of planktic foraminifera. Although faunal assemblage data available have their own limits, it is reasonable to assume that the foraminiferal assemblage in the NEC (10°N–20°N) region, manifested by those of P1, PC17 and PC20 sites (Figure 1a), would prevail north of the thermocline ridge (ca. 7°N–9°N) between the NECC and NEC (Figures 1b and 1c). If this was the case, our foraminiferal assemblage data indicate that the oceanographic features of the NEC region had prevailed at the study site (6°40′N) during the last deglaciation. This implies that, if the zonal surface current system had not been significantly different from that of the present day, then the ITCZ-NECC system, being located over the study site at present, and the thermocline ridge would have been located at least 2° southward during the last deglaciation. Our minimum estimate is slightly greater than the previously suggested mean annual displacement of about 1.5° during the HS1, which was projected using model simulations [*McGee et al*., 2014]. Further research along a meridional transect is therefore required to investigate the magnitude of these latitudinal movements.

6. Conclusions

Comparison of the measured δ^{18}O with the predicted calcite δ^{18}O indicated a calcification depth of 70–100 m for *G. sacculifer*, 120–140 m for *P. obliquiloculata*, and 160–200 m depth for *G. tumida* during the late

Holocene at the study site. We infer that the Mg/Ca-derived temperatures of each species represent the temperatures in the mixed layer, upper thermocline, and lower thermocline, respectively.

Our results suggest that the vertical temperature gradient between the dwelling depths of *P. obliquiloculata* and *G. sacculifer* was smaller during the last deglaciation than during the preceding and the following periods. This feature occurred without changes in the lower thermocline temperatures and can be explained only by more similar depth habitats between the two species, which likely resulted from a weakening of water column stratification above the upper part of the thermocline.

The faunal assemblages of planktic foraminifera during the last deglaciation are similar to those of the present-day subtropical central Pacific sites (15°N and 21°N) that lie under the strong influence of the northeasterly trade winds and the NEC. This raises the possibility that the study site, being under the control of the ITCZ-NECC system at present, was under the direct influence of the northeasterly trade winds and NEC during the 18–12 ka interval, indicating in turn that the ITCZ was situated south of the study site during this period. Our interpretation is consistent with previous studies that suggest a southerly position of the ITCZ during two prominent NH cooling events; i.e., HS1 and YD, although the temporal resolution of our record does not resolve the millennial scale climate variability of the last deglaciation. Based on planktic foraminifera assemblages, we hypothesize that the ITCZ-NECC system, being located over the study site at present, would have been displaced at least 2° southward during these events.

Acknowledgments
This work was supported by the Ministry of Oceans and Fisheries, Republic of Korea (PM 59352 and PM 59331), KIOST (PE99456), and by the SNU-SEES BK 21 program. Authors thank Y. Yokoyama, the editor, M. Mohtadi and an anonymous reviewer for comments that improved the quality of this manuscript. The data set is archived in supporting information Tables S1 and S2.

References

Anand, P., H. Elderfield, and M. H. Conte (2003), Calibration of Mg/Ca thermometry in planktonic foraminifera from a sediment trap time series, *Paleoceanography*, *18*(2), 1050, doi:10.1029/2002PA000846.

Andreasen, D. J., and A. C. Ravelo (1997), Tropical Pacific Ocean thermocline depth reconstructions for the Last Glacial Maximum, *Paleoceanography*, *12*(3), 395–413, doi:10.1029/97PA00822.

Ayliffe, L. K., et al. (2013), Rapid interhemispheric climate links via the Australasian monsoon during the last deglaciation, *Nat. Commun.*, *4*, 2908, doi:10.1038/ncomms3908.

Bé, A. W. H. (1980), Gametogenic calcification in a spinose planktonic foraminifer, *Globigerinoides sacculifer* (Brady), *Mar. Micropaleontol.*, *5*, 283–310, doi:10.1016/0377-8398(80)90014-6.

Bard, E., F. Rostek, J.-L. Turon, and S. Gendreau (2000), Hydrological impact of heinrich events in the subtropical northeast Atlantic, *Science*, *289*(5483), 1321–1324, doi:10.1126/science.289.5483.1321.

Barker, S., M. Greaves, and H. Elderfield (2003), A study of cleaning procedures used for foraminiferal Mg/Ca paleothermometry, *Geochem. Geophys. Geosyst.*, *4*(9), 8407, doi:10.1029/2003GC000559.

Barker, S., P. Diz, M. J. Vautravers, J. Pike, G. Knorr, I. R. Hall, and W. S. Broecker (2009), Interhemispheric Atlantic seesaw response during the last deglaciation, *Nature*, *457*(7233), 1097–1102, doi:10.1038/nature07770.

Benway, H. M., A. C. Mix, B. A. Haley, and G. P. Klinkhammer (2006), Eastern Pacific Warm Pool paleosalinity and climate variability: 0–30 kyr, *Paleoceanography*, *21*, PA3008, doi:10.1029/2005PA001208.

Berger, W. H. (1977), Deep-sea carbonate and the deglaciation preservation spike in pteropods and foraminifera, *Nature*, *269*(5626), 301–304, doi:10.1038/269301a0.

Bianchi, C., and R. Gersonde (2004), Climate evolution at the last deglaciation: The role of the Southern Ocean, *Earth Planet. Sci. Lett.*, *228*(3–4), 407–424, doi:10.1016/j.epsl.2004.10.003.

Bijma, J., and C. Hemleben (1994), Population dynamics of the planktic foraminifer *Globigerinoides sacculifer* (Brady) from the central Red Sea, *Deep Sea Res., Part I*, *41*(3), 485–510, doi:10.1016/0967-0637(94)90092-2.

Black, D. E., R. C. Thunell, and E. J. Tappa (2001), Planktonic foraminiferal response to the 1997–1998 El Niño: A sediment-trap record from the Santa Barbara Basin, *Geology*, *29*(12), 1075–1078, doi:10.1130/0091-7613(2001)029 < 1075:PFRTTE>2.0.CO;2.

Bostock, H. C., et al. (2013), A review of the Australian-New Zealand sector of the Southern Ocean over the last 30 ka (Aus-INTIMATE project), *Quat. Sci. Rev.*, *74*, 35–57, doi:10.1016/j.quascirev.2012.07.018.

Bova, S. C., T. Herbert, Y. Rosenthal, J. Kalansky, M. Altabet, C. Chazen, A. Mojarro, and J. Zech (2015), Links between eastern equatorial Pacific stratification and atmospheric CO_2 rise during the last deglaciation, *Paleoceanography*, *30*, 1407–1424, doi:10.1002/2015PA002816.

Brown, S. J., and H. Elderfield (1996), Variations in Mg/Ca and Sr/Ca ratios of planktonic foraminifera caused by postdepositional dissolution: Evidence of shallow Mg-dependent dissolution, *Paleoceanography*, *11*(5), 543–551, doi:10.1029/96PA01491.

Calvo, E., C. Pelejero, P. De Deckker, and G. A. Logan (2007), Antarctic deglacial pattern in a 30 kyr record of sea surface temperature offshore South Australia, *Geophys. Res. Lett.*, *34*, L13707, doi:10.1029/2007GL029937.

Calvo, E., C. Pelejero, L. D. Pena, I. Cacho, and G. A. Logan (2011), Eastern Equatorial Pacific productivity and related-CO_2 changes since the last glacial period, *Proc. Natl. Acad. Sci. U. S. A.*, *108*(14), 5537–5541, doi:10.1073/pnas.1009761108.

Caromel, A. G. M., D. N. Schmidt, J. C. Phillips, and E. J. Rayfield (2014), Hydrodynamic constraints on the evolution and ecology of planktic foraminifera, *Mar. Micropaleontol.*, *106*, 69–78, doi:10.1016/j.marmicro.2014.01.002.

Chang, Y.-P., W.-L. Wang, Y. Yokoyama, H. Matsuzaki, H. Kawahata, and M.-T. Chen (2008), Millennial-scale planktic foraminifer faunal variability in the East China Sea during the past 40000 years (IMAGES MD012404 from the Okinawa Trough), *Terr. Atmos. Oceanic Sci.*, *19*(4), 389–401.

Cléroux, C., E. Cortijo, P. Anand, L. Labeyrie, F. Bassinot, N. Caillon, and J.-C. Duplessy (2008), Mg/Ca and Sr/Ca ratios in planktonic foraminifera: Proxies for upper water column temperature reconstruction, *Paleoceanography*, *23*, PA3214, doi:10.1029/2007PA001505.

Conroy, J. L., K. M. Cobb, J. Lynch-Stieglitz, and P. J. Polissar (2014), Constraints on the salinity-oxygen isotope relationship in the central tropical Pacific Ocean, *Mar. Chem.*, *161*, 26–33, doi:10.1016/j.marchem.2014.02.001.

Coxall, H. K., P. N. Pearson, N. J. Shackleton, and M. A. Hall (2000), Hantkeninid depth adaptation: An evolving life strategy in a changing ocean, *Geology*, *28*(1), 87–90, doi:10.1130/0091-7613(2000)28 < 87:HDAAEL>2.0.CO;2.

de Garidel-Thoron, T., Y. Rosenthal, L. Beaufort, E. Bard, C. Sonzogni, and A. C. Mix (2007), A multiproxy assessment of the western equatorial Pacific hydrography during the last 30 kyr, *Paleoceanography*, *22*, PA3204, doi:10.1029/2006PA001269.

Dekens, P. S., D. W. Lea, D. K. Pak, and H. J. Spero (2002), Core top calibration of Mg/Ca in tropical foraminifera: Refining paleotemperature estimation, *Geochem. Geophys. Geosyst.*, *3*(4), 1–29, doi:10.1029/2001GC000200.

Denton, G. H., R. F. Anderson, J. R. Toggweiler, R. L. Edwards, J. M. Schaefer, and A. E. Putnam (2010), The Last Glacial Termination, *Science*, *328*(5986), 1652–1656, doi:10.1126/science.1184119.

Donguy, J.-R., and G. Meyers (1996), Mean annual variation of transport of major currents in the tropical Pacific Ocean, *Deep Sea Res., Part I*, *43*(7), 1105–1122, doi:10.1016/0967-0637(96)00047-7.

Eldin, G., and M. Rodier (2003), Ocean physics and nutrient fields along 180° during an El Niño-Southern Oscillation cold phase, *J. Geophys. Res.*, *108*(C12), 8137, doi:10.1029/2000JC000746.

Erez, J., and S. Honjo (1981), Oxygen and Carbon Isotopes in Foraminifera Comparison of isotopic composition of planktonic foraminifera in plankton tows, sediment traps and sediments, *Palaeogeogr. Palaeoclimatol. Palaeoecol.*, *33*(1), 129–156, doi:10.1016/0031-0182(81)90035-3.

Fairbanks, R. G., and P. H. Wiebe (1980), Foraminifera and chlorophyll maximum: Vertical distribution, seasonal succession, and paleoceanographic significance, *Science*, *209*(4464), 1524–1526, doi:10.1126/science.209.4464.1524.

Farmer, E. C., A. Kaplan, P. B. de Menocal, and J. Lynch-Stieglitz (2007), Corroborating ecological depth preferences of planktonic foraminifera in the tropical Atlantic with the stable oxygen isotope ratios of core top specimens, *Paleoceanography*, *22*, PA3205, doi:10.1029/2006PA001361.

Gibbons, F. T., D. W. Oppo, M. Mohtadi, Y. Rosenthal, J. Cheng, Z. Liu, and B. K. Linsley (2014), Deglacial $\delta^{18}O$ and hydrologic variability in the tropical Pacific and Indian Oceans, *Earth Planet. Sci. Lett.*, *387*, 240–251, doi:10.1016/j.epsl.2013.11.032.

Guilderson, T. P., D. P. Schrag, M. Kashgarian, and J. Southon (1998), Radiocarbon variability in the western equatorial Pacific inferred from a high-resolution coral record from Nauru Island, *J. Geophys. Res.*, *103*(C11), 24,641–24,650, doi:10.1029/98JC02271.

Haug, G. H., K. A. Hughen, D. M. Sigman, L. C. Peterson, and U. Röhl (2001), Southward migration of the intertropical convergence zone through the holocene, *Science*, *293*(5533), 1304–1308, doi:10.1126/science.1059725.

Hemleben, C., M. Spindler, I. Breitinger, and R. Ott (1987), Morphological and physiological responses of *Globigerinoides sacculifer* (Brady) under varying laboratory conditions, *Mar. Micropaleontol.*, *12*, 305–324, doi:10.1016/0377-8398(87)90025-9.

Hemleben, C., M. Spindler, and O. R. Anderson (1989), Ecology, in *Modern Planktonic Foraminifera*, edited by C. Hemleben, M. Spindler, and O. R. Anderson, pp. 220–257, Springer, N. Y., doi:10.1007/978-1-4612-3544-6_10.

Hemming, S. R. (2004), Heinrich events: Massive late Pleistocene detritus layers of the North Atlantic and their global climate imprint, *Rev. Geophys.*, *42*, RG1005, doi:10.1029/2003RG000128.

Huang, C.-Y., S.-F. Wu, M. Zhao, M.-T. Chen, C.-H. Wang, X. Tu, and P. B. Yuan (1997), Surface ocean and monsoon climate variability in the South China Sea since the last glaciation, *Mar. Micropaleontol.*, *32*(1–2), 71–94, doi:10.1016/S0377-8398(97)00014-5.

Kaplan, M. R., J. M. Schaefer, G. H. Denton, D. J. A. Barrell, T. J. H. Chinn, A. E. Putnam, B. G. Andersen, R. C. Finkel, R. Schwartz, and A. M. Doughty (2010), Glacier retreat in New Zealand during the Younger Dryas stadial, *Nature*, *467*(7312), 194–197, doi:10.1038/nature09313.

Kawahata, H., A. Nishimura, and M. K. Gagan (2002), Seasonal change in foraminiferal production in the western equatorial Pacific warm pool: Evidence from sediment trap experiments, *Deep Sea Res., Part II*, *49*(13–14), 2783–2800, doi:10.1016/S0967-0645(02)00058-9.

Kennett, J. P., and M. S. Srinivasan (1983), *Neogene Planktonic Foraminifera: A Phylogenetic Atlas*, xv, 265 pp., Hutchinson Ross; distributed worldwide by Van Nostrand Reinhold, Stroudsburg, Pa.

Kienast, M., S. Steinke, K. Stattegger, and S. E. Calvert (2001), Synchronous Tropical South China Sea SST change and Greenland warming during deglaciation, *Science*, *291*(5511), 2132–2134, doi:10.1126/science.1057131.

Kienast, M., S. S. Kienast, S. E. Calvert, T. I. Eglinton, G. Mollenhauer, R. Francois, and A. C. Mix (2006), Eastern Pacific cooling and Atlantic overturning circulation during the last deglaciation, *Nature*, *443*(7113), 846–849, doi:10.1038/nature05222.

Kienast, S. S., T. Friedrich, N. Dubois, P. S. Hill, A. Timmermann, A. C. Mix, and M. Kienast (2013), Near collapse of the meridional SST gradient in the eastern equatorial Pacific during Heinrich Stadial 1, *Paleoceanography*, *28*, 663–674, doi:10.1002/2013PA002499.

Kim, S.-T., and J. R. O'Neil (1997), Equilibrium and nonequilibrium oxygen isotope effects in synthetic carbonates, *Geochim. Cosmochim. Acta*, *61*(16), 3461–3475, doi:10.1016/S0016-7037(97)00169-5.

Kimoto, K., H. Takaoka, M. Oda, M. Ikehara, H. Matsuoka, M. Okada, T. Oba, and A. Taira (2003), Carbonate dissolution and planktonic foraminiferal assemblages observed in three piston cores collected above the lysocline in the western equatorial Pacific, *Mar. Micropaleontol.*, *47*(3–4), 227–251, doi:10.1016/S0377-8398(02)00118-4.

Koutavas, A., and J. P. Sachs (2008), Northern timing of deglaciation in the eastern equatorial Pacific from alkenone paleothermometry, *Paleoceanography*, *23*, PA4205, doi:10.1029/2008PA001593.

Kubota, K., Y. Yokoyama, T. Ishikawa, S. Obrochta, and A. Suzuki (2014), Larger CO_2 source at the equatorial Pacific during the last deglaciation, *Sci. Rep.*, *4*, 5261, doi:10.1038/srep05261.

Lamy, F., J. Kaiser, U. Ninnemann, D. Hebbeln, H. W. Arz, and J. Stoner (2004), Antarctic timing of surface water changes off Chile and Patagonian Ice sheet response, *Science*, *304*(5679), 1959–1962, doi:10.1126/science.1097863.

Lamy, F., J. Kaiser, H. W. Arz, D. Hebbeln, U. Ninnemann, O. Timm, A. Timmermann, and J. R. Toggweiler (2007), Modulation of the bipolar seesaw in the Southeast Pacific during Termination 1, *Earth Planet. Sci. Lett.*, *259*(3–4), 400–413, doi:10.1016/j.epsl.2007.04.040.

Le, J., and R. C. Thunell (1996), Modelling planktic foraminiferal assemblage changes and application to sea surface temperature estimation in the western equatorial Pacific Ocean, *Mar. Micropaleontol.*, *28*(3–4), 211–229, doi:10.1016/0377-8398(96)00009-6.

Le Bouteiller, A., A. Leynaert, M. R. Landry, R. Le Borgne, J. Neveux, M. Rodier, J. Blanchot, and S. L. Brown (2003), Primary production, new production, and growth rate in the equatorial Pacific: Changes from mesotrophic to oligotrophic regime, *J. Geophys. Res.*, *108*(C12), 8141, doi:10.1029/2001JC000914.

Lea, D. W., T. A. Mashiotta, and H. J. Spero (1999), Controls on magnesium and strontium uptake in planktonic foraminifera determined by live culturing, *Geochim. Cosmochim. Acta*, *63*(16), 2369–2379, doi:10.1016/S0016-7037(99)00197-0.

Lea, D. W., D. K. Pak, C. L. Belanger, H. J. Spero, M. A. Hall, and N. J. Shackleton (2006), Paleoclimate history of Galápagos surface waters over the last 135,000 yr, *Quat. Sci. Rev.*, *25*(11–12), 1152–1167, doi:10.1016/j.quascirev.2005.11.010.

Leduc, G., L. Vidal, K. Tachikawa, and E. Bard (2009), ITCZ rather than ENSO signature for abrupt climate changes across the tropical Pacific?, *Quat. Res.*, *72*(1), 123–131, doi:10.1016/j.yqres.2009.03.006.

Lee, K. E., N. C. Slowey, and T. D. Herbert (2001), Glacial sea surface temperatures in the subtropical North Pacific: A comparison of U37 k′, δ18O, and foraminiferal assemblage temperature estimates, *Paleoceanography*, *16*(3), 268–279, doi:10.1029/1999PA000493.

Leech, P. J., J. Lynch-Stieglitz, and R. Zhang (2013), Western Pacific thermocline structure and the Pacific marine Intertropical Convergence Zone during the Last Glacial Maximum, *Earth Planet. Sci. Lett.*, *363*, 133–143, doi:10.1016/j.epsl.2012.12.026.

Legates, D. R., and C. J. Willmott (1990), Mean seasonal and spatial variability in gauge-corrected, global precipitation, *Int. J. Climatol.*, *10*(2), 111–127, doi:10.1002/joc.3370100202.

Locarnini, R. A., et al. (2013), World Ocean Atlas 2013, in *Temperature, NOAA Atlas NESDIS 72*, vol. 1, edited by S. Levitus, 40 pp., Silver Spring, Md.

Lynch-Stieglitz, J., et al. (2015), Glacial-interglacial changes in central tropical Pacific surface seawater property gradients, *Paleoceanography*, *30*, 423–438, doi:10.1002/2014PA002746.

Marcos, A., and S. J. Hill (2000), A drift correction procedure for ICP-AES systems, *Analyst*, *125*(6), 1015–1020, doi:10.1039/B002408M.

Masunaga, H., and T. S. L'Ecuyer (2010), Equatorial asymmetry of the East Pacific ITCZ: Observational constraints on the underlying processes, *J. Clim.*, *24*(6), 1784–1800, doi:10.1175/2010JCLI3854.1.

McGee, D., A. Donohoe, J. Marshall, and D. Ferreira (2014), Changes in ITCZ location and cross-equatorial heat transport at the Last Glacial Maximum, Heinrich Stadial 1, and the mid-Holocene, *Earth Planet. Sci. Lett.*, *390*, 69–79, doi:10.1016/j.epsl.2013.12.043.

Medina-Elizalde, M., and D. W. Lea (2005), The Mid-Pleistocene transition in the Tropical Pacific, *Science*, *310*(5750), 1009–1012, doi:10.1126/science.1115933.

Mekik, F. A., R. F. Anderson, P. Loubere, R. François, and M. Richaud (2012), The mystery of the missing deglacial carbonate preservation maximum, *Quat. Sci. Rev.*, *39*, 60–72, doi:10.1016/j.quascirev.2012.01.024.

Mohtadi, M., P. Rossel, C. B. Lange, S. Pantoja, P. Böning, D. J. Repeta, M. Grunwald, F. Lamy, D. Hebbeln, and H.-J. Brumsack (2008), Deglacial pattern of circulation and marine productivity in the upwelling region off central-south Chile, *Earth Planet. Sci. Lett.*, *272*(1–2), 221–230, doi:10.1016/j.epsl.2008.04.043.

Mohtadi, M., D. W. Oppo, S. Steinke, J.-B. W. Stuut, R. De Pol-Holz, D. Hebbeln, and A. Luckge (2011a), Glacial to Holocene swings of the Australian-Indonesian monsoon, *Nat. Geosci.*, *4*(8), 540–544, doi:10.1038/ngeo1209.

Mohtadi, M., D. W. Oppo, A. Lückge, R. DePol-Holz, S. Steinke, J. Groeneveld, N. Hemme, and D. Hebbeln (2011b), Reconstructing the thermal structure of the upper ocean: Insights from planktic foraminifera shell chemistry and alkenones in modern sediments of the tropical eastern Indian Ocean, *Paleoceanography*, *26*, PA3219, doi:10.1029/2011PA002132.

Mohtadi, M., M. Prange, D. W. Oppo, R. De Pol-Holz, U. Merkel, X. Zhang, S. Steinke, and A. Luckge (2014), North Atlantic forcing of tropical Indian Ocean climate, *Nature*, *509*(7498), 76–80, doi:10.1038/nature13196.

Montade, V., M. Kageyama, N. Combourieu-Nebout, M.-P. Ledru, E. Michel, G. Siani, and C. Kissel (2015), Teleconnection between the Intertropical Convergence Zone and southern westerly winds throughout the last deglaciation, *Geology*, *43*(8), 735–738, doi:10.1130/g36745.1.

Nürnberg, D., J. Bijma, and C. Hemleben (1996), Assessing the reliability of magnesium in foraminiferal calcite as a proxy for water mass temperatures, *Geochim. Cosmochim. Acta*, *60*(5), 803–814, doi:10.1016/0016-7037(95)00446-7.

Nürnberg, D., T. Böschen, K. Doering, E. Mollier-Vogel, J. Raddatz, and R. Schneider (2015), Sea surface and subsurface circulation dynamics off equatorial Peru during the last ~17 kyr, *Paleoceanography*, *30*, 984–999, doi:10.1002/2014PA002706.

Oppo, D. W., and Y. Sun (2005), Amplitude and timing of sea-surface temperature change in the northern South China Sea: Dynamic link to the East Asian monsoon, *Geology*, *33*(10), 785–788, doi:10.1130/g21867.1.

Pahnke, K., J. P. Sachs, L. Keigwin, A. Timmermann, and S.-P. Xie (2007), Eastern tropical Pacific hydrologic changes during the past 27,000 years from D/H ratios in alkenones, *Paleoceanography*, *22*, PA4214, doi:10.1029/2007PA001468.

Palmer, M. R., and P. N. Pearson (2003), A 23,000-year record of surface water pH and PCO_2 in the Western Equatorial Pacific Ocean, *Science*, *300*(5618), 480–482, doi:10.1126/science.1080796.

Parrenin, F., V. Masson-Delmotte, P. Köhler, D. Raynaud, D. Paillard, J. Schwander, C. Barbante, A. Landais, A. Wegner, and J. Jouzel (2013), Synchronous change of atmospheric CO_2 and Antarctic temperature during the last deglacial warming, *Science*, *339*(6123), 1060–1063, doi:10.1126/science.1226368.

Partin, J. W., K. M. Cobb, J. F. Adkins, B. Clark, and D. P. Fernandez (2007), Millennial-scale trends in west Pacific warm pool hydrology since the Last Glacial Maximum, *Nature*, *449*(7161), 452–455, doi:10.1038/nature06164.

Patrick, A., and R. C. Thunell (1997), Tropical Pacific sea surface temperatures and upper water column thermal structure during the Last Glacial Maximum, *Paleoceanography*, *12*(5), 649–657, doi:10.1029/97PA01553.

Peterson, L. C., G. H. Haug, K. A. Hughen, and U. Röhl (2000), Rapid changes in the hydrologic cycle of the Tropical Atlantic during the last glacial, *Science*, *290*(5498), 1947–1951, doi:10.1126/science.290.5498.1947.

Rashid, H., and E. A. Boyle (2007), Mixed-layer deepening during heinrich events: A multi-planktonic foraminiferal $\delta^{18}O$ approach, *Science*, *318*(5849), 439–441, doi:10.1126/science.1146138.

Regenberg, M., A. Regenberg, D. Garbe-Schönberg, and D. W. Lea (2014), Global dissolution effects on planktonic foraminiferal Mg/Ca ratios controlled by the calcite-saturation state of bottom waters, *Paleoceanography*, *29*, 127–142, doi:10.1002/2013PA002492.

Reimer, P. J., et al. (2013), IntCal13 and Marine13 radiocarbon age calibration curves 0–50,000 years cal BP, *Radiocarbon*, *55*(4), 1869–1887, doi:10.2458/azu_js_rc.55.16947.

Rickaby, R. E. M., and P. Halloran (2005), Cool La Niña during the warmth of the Pliocene?, *Science*, *307*(5717), 1948–1952, doi:10.1126/science.1104666.

Riforgiato, F. (2013), Revision of the Messinian-Early Zanclean sediments from ODP Hole 953C (Canary Island Archipelago, North-Eastern Atlantic): Biostratigraphy, cyclostratigraphy, and astronomical tuning, *Paleontol. J.*, *2013*, 1–17, doi:10.1155/2013/947839.

Rincón-Martínez, D., S. Steph, F. Lamy, A. Mix, and R. Tiedemann (2011), Tracking the equatorial front in the eastern equatorial Pacific Ocean by the isotopic and faunal composition of planktonic foraminifera, *Mar. Micropaleontol.*, *79*(1–2), 24–40, doi:10.1016/j.marmicro.2011.01.001.

Romero, O. E., J.-H. Kim, and D. Hebbeln (2006), Paleoproductivity evolution off central Chile from the Last Glacial Maximum to the Early Holocene, *Quat. Res.*, *65*(3), 519–525, doi:10.1016/j.yqres.2005.07.003.

Sagawa, T., Y. Yokoyama, M. Ikehara, and M. Kuwae (2012), Shoaling of the western equatorial Pacific thermocline during the last glacial maximum inferred from multispecies temperature reconstruction of planktonic foraminifera, *Palaeogeogr. Palaeoclimatol. Palaeoecol.*, *346–347*, 120–129, doi:10.1016/j.palaeo.2012.06.002.

Saitō, T., D. Breger, and P. R. Thompson (1981), *Systematic Index of Recent and Pleistocene Planktonic Foraminifera*, 190 pp., Univ. of Tokyo Press, Tokyo.

Schrag, D. P. (1999), Rapid analysis of high-precision Sr/Ca ratios in corals and other marine carbonates, *Paleoceanography*, *14*(2), 97–102, doi:10.1029/1998PA900025.

Shakun, J. D., P. U. Clark, F. He, S. A. Marcott, A. C. Mix, Z. Liu, B. Otto-Bliesner, A. Schmittner, and E. Bard (2012), Global warming preceded by increasing carbon dioxide concentrations during the last deglaciation, *Nature*, *484*(7392), 49–54, doi:10.1038/nature10915.

Spencer, R. W. (1993), Global oceanic precipitation from the MSU during 1979–91 and comparisons to other climatologies, *J. Clim.*, *6*(7), 1301–1326, doi:10.1175/1520-0442(1993)006 < 1301:GOPFTM>2.0.CO;2.
Stenni, B., et al. (2011), Expression of the bipolar see-saw in Antarctic climate records during the last deglaciation, *Nat. Geosci.*, *4*(1), 46–49, doi:10.1038/ngeo1026.
Stott, L., A. Timmermann, and R. Thunell (2007), Southern hemisphere and deep-sea warming led deglacial atmospheric CO_2 rise and tropical warming, *Science*, *318*(5849), 435–438, doi:10.1126/science.1143791.
Stuiver, M., and P. J. Reimer (1993), Extended ^{14}C data base and revised CALIB 3.0 ^{14}C age calibration program, *Radiocarbon*, *35*, 215–230.
Thunell, R. C., and S. Honjo (1981a), Calcite dissolution and the modification of planktonic foraminiferal assemblages, *Mar. Micropaleontol.*, *6*(2), 169–182, doi:10.1016/0377-8398(81)90004-9.
Thunell, R. C., and S. Honjo (1981b), Planktonic foraminiferal flux to the deep ocean: Sediment trap results from the tropical Atlantic and the central Pacific, *Mar. Geol.*, *40*(3), 237–253, doi:10.1016/0025-3227(81)90142-0.
Thunell, R. C., and L. A. Reynolds (1984), Sedimentation of planktonic foraminifera: Seasonal changes in species flux in the Panama Basin, *Micropaleontology*, *30*(3), 243–262, doi:10.2307/1485688.
Timmermann, A., J. Sachs, and O. E. Timm (2014), Assessing divergent SST behavior during the last 21 ka derived from alkenones and *G. ruber*-Mg/Ca in the equatorial Pacific, *Paleoceanography*, *29*, 680–696, doi:10.1002/2013PA002598.
Ujiie, Y., and H. Ujiie (2000), Distribution and oceanographic relationships of modern planktonic foraminifera in the Ryukyu Arc region, northwest Pacific ocean, *J. Foraminiferal Res.*, *30*(4), 336–360, doi:10.2113/0300336.
Veres, D., et al. (2013), The Antarctic ice core chronology (AICC2012): An optimized multi-parameter and multi-site dating approach for the last 120 thousand years, *Clim. Past*, *9*(4), 1733–1748, doi:10.5194/cp-9-1733-2013.
Visser, K., R. Thunell, and L. Stott (2003), Magnitude and timing of temperature change in the Indo-Pacific warm pool during deglaciation, *Nature*, *421*, 152–155, doi:10.1038/nature01297.
Wang, Y. J., H. Cheng, R. L. Edwards, Z. S. An, J. Y. Wu, C.-C. Shen, and J. A. Dorale (2001), A high-resolution absolute-dated Late Pleistocene Monsoon record from Hulu Cave, China, *Science*, *294*(5550), 2345–2348, doi:10.1126/science.1064618.
Yamasaki, M., A. Sasaki, M. Oda, and H. Domitsu (2008), Western equatorial Pacific planktic foraminiferal fluxes and assemblages during a La Niña year (1999), *Mar. Micropaleontol.*, *66*(3–4), 304–319, doi:10.1016/j.marmicro.2007.10.006.
Zweng, M. M., et al. (2013), *World Ocean Atlas 2013*, in *Salinity, NOAA Atlas NESDIS 72*, vol. 2, edited by S. Levitus, 39 pp., Silver Spring, Md.

Erratum

In the originally published version of this article, the author names were incorrectly typeset. The error has since been corrected and this version may be considered the authoritative version of record.